Comparison of Three Ternary Lipid Bilayer Mixtures: FRET and ESR Reveal Nanodomains

Frederick A. Heberle,[†] Jing Wu,[†] Shih Lin Goh,[‡] Robin S. Petruzielo,[§] and Gerald W. Feigenson[†*]
[†]Department of Molecular Biology and Genetics, Field of Biophysics, [‡]Field of Biochemistry, Molecular and Cell Biology, and [§]Department of Physics, Cornell University, Ithaca, New York

ABSTRACT   Phase diagrams of ternary lipid mixtures containing cholesterol have provided valuable insight into cell membrane behaviors, especially by describing regions of coexisting liquid-disordered (Ld) and liquid-ordered (Lo) phases. Fluorescence microscopy imaging of giant unilamellar vesicles has greatly assisted the determination of phase behavior in these systems. However, the requirement for optically resolved Ld + Lo domains can lead to the incorrect inference that in lipid-only mixtures, Ld + Lo domain coexistence generally shows macroscopic domains. Here we show this inference is incorrect for the low melting temperature phosphatidylcholines abundant in mammalian plasma membranes. By use of high compositional resolution Förster resonance energy transfer measurements, together with electron spin resonance data and spectral simulation, we find that ternary mixtures of DSPC and cholesterol together with either POPC or SOPC, do indeed have regions of Ld + Lo coexistence. However, phase domains are much smaller than the optical resolution limit, likely on the order of the Förster distance for energy transfer (R_0, ~2–8 nm).

INTRODUCTION

What is the connection between the membrane properties of living cells, and chemically simplified model bilayer mixtures?

While the physical chemical behaviors of even simplified lipid bilayer mixtures are not fully understood, complex membranes of living cells have provided important clues to the underlying physical properties of bilayers. The functional lipid raft, a compositionally distinct membrane domain, is now thought to play a role in normal cell functions including signaling, membrane transport and protein sorting, and virus pathogenesis (1). These characteristics of biological membranes suggest highly nonuniform mixing of membrane components.

We ask, what are the sizes, shapes, lifetimes, connectivities, and partitioning behaviors of membrane heterogeneities? Are proteins required for raft formation?

Such descriptions are important, as many functions ascribed to rafts require the existence of domains large enough to accommodate several proteins, and stable for at least the time required for proteins to find each other and interact (2). Measurements of raft size in resting cells have resulted in estimates from a few to hundreds of nanometers (3), underscoring the difficulty of teasing apart mechanisms that mediate domain size in an experimental system as complex, dynamic, and variable as the plasma membrane (PM).

Model lipid bilayers offer a measure of simplification to the problem. Model bilayers can be chemically well defined and systematically studied within the powerful framework of equilibrium thermodynamics. Indeed, model studies have figured prominently in the development of the raft hypothesis by providing a picture of PM domains as coexisting liquid-disordered (Ld) and liquid-ordered (Lo) phases. The minimal requirement for liquid phase coexistence in model systems, met by all animal cell PMs, is a ternary mixture of cholesterol, low-, and high-melting temperature (T_M) lipids (4). Furthermore, the low-T_M lipid seems to be an important factor in controlling liquid phase domain size. The well-studied low-T_M lipids DOPC (1,2-dioleoyl-sn-glycero-3-phosphocholine) and DPhPC (1,2-diphytanoyl-sn-glycero-3-phosphocholine), though rare in mammalian PM, exhibit micron-sized domains in ternary mixtures (5,6).

In contrast, biologically abundant low-T_M lipids including POPC (1-palmitoyl-2-oleoyl-sn-glycero-3-phosphocholine) and SOPC (1-stearoyl-2-oleoyl-sn-glycero-3-phosphocholine) do not (7–9), though methods sensitive to submicron length scales consistently indicate liquid phase heterogeneity in POPC- and SOPC-containing ternary mixtures (7,8,10,11). Driven by these reports, a growing theoretical literature seeks to explain submicron domains in lipid-only bilayers in terms of composition-dependent membrane properties like line tension and bending stiffness (12,13). Theoretical treatments have indeed outpaced experiments, largely due to the difficulty of obtaining reliable data at length scales below the optical resolution limit (3). Composition-dependent data are particularly valuable, because composition is the primary mechanism by which a cell can alter membrane phase behavior. These data are also challenging to acquire: Precise control of membrane composition is laborious, and the effect of small, systematic changes in membrane composition on domain properties remains largely unexplored.

Förster resonance energy transfer measurements (FRET) between diffusing lipid fluorophores (SP-FRET (14)) is sensitive to membrane domains larger than R_0 (typically 2–8 nm). To address the effect of bilayer composition on domain size, we measured SP-FRET over the entire composition space of the ternary systems DSPC (1,2-distearoyl-*sn*-glycero-3-phosphocholine)/DOPC/chol, DSPC/POPC/chol, and DSPC/SOPC/chol. The first of these mixtures, well established as exhibiting first-order Ld + Lo phase coexistence with clearly-defined phase boundaries, provides a standard for comparison (6).

We report that the latter two systems show FRET and electron spin resonance (ESR) behavior remarkably similar to that seen in DSPC/DOPC/chol. This behavior is described by probe partitioning between phases and the Lever rule (14), even at compositions where giant unilamellar vesicle (GUV) images appear uniform. Apparently, nanoscopic liquid domains in these systems behave closely enough to genuine phases that they may be usefully described by the tools of equilibrium thermodynamics.

MATERIALS AND METHODS

Materials

Phospholipids were from Avanti Polar Lipids (Alabaster, AL), and the cholesterol was from Nu Chek Prep (Elysian, MN). Fluorescent dyes BoDIPY-PC (2-(4,4-difluoro-5,7-dimethyl-4-bora-3a,4a-diaza-s-indacene-3-pentanoyl)-1-hexadecanoyl-*sn*-glycero-3-phosphocholine) and Fast-DiI (1,1′-dilinoleyl-3,3,3′,3′-tetramethylindocarbocyanine perchlorate) were from Invitrogen (Carlsbad, CA). DHE (Ergosta-5,7,9(11),22-tetraen-3β-ol) was from Sigma-Aldrich (St. Louis, MO).

Spin-labeled lipid 16-PC (1-palmitoyl-2-(16-doxyl stearoyl) phosphatidylcholine) was a gift from Boris Dzikovski of the National Biomedical Center for Advanced ESR Technology at Cornell University. Purity of >99% was confirmed by thin-layer chromatography (TLC) on washed, activated Adsorbosil TLC plates (Alltech, Deerfield, IL), developed with chloroform/methanol/water (C/M/W) 65:25:4 for phospholipids, 65:35:4 for 16-PC, C/M 9:1 for Fast-DiI, and petroleum ether/diethyl ether/chloroform 7:3:3 for cholesterol. Solvents were HPLC grade. Concentration of phospholipid stocks was determined to <1% by inorganic phosphate assay, and of fluorescent dye stocks by absorption spectroscopy using an HP 8452A spectrophotometer (Hewlett-Packard, Palo Alto, CA). Cholesterol stocks were prepared by standard gravimetric methods to ~0.2%.

FRET sample preparation

Chloroform mixtures of lipids in 2% compositional increments were prepared in glass culture tubes using a syringe and repeating dispenser (Hamilton USA, Reno, NV). Samples received a fixed volume of a combined chloroform stock of fluorescent probes to achieve probe/lipid mole ratios of ~1:200 (DHE), 1:1500 (BoDIPY-PC), and 1:3000 (Fast-DiI). Multilamellar vesicles were prepared from these mixtures using rapid solvent exchange (RSE (15)) as previously described (6). After measurement, randomly selected samples were analyzed by TLC and showed no evidence of breakdown.

Fluorescence data were collected at 22°C with a F7000 spectrofluorimeter (Hitachi High Technologies America, Schaumburg, IL). A 100 μL sample aliquot was diluted into 1.90 mL RSE buffer (200 mM KC1, 5 mM PIPES, 1mM EDTA) by gently stirring in a cuvette. Intensity (2.5 nm bandpass for excitation and emission slits, 10 s integration time) was measured in six channels (excitation/emission λ, nm):

DHE fluorescence (327/393),
BoDIPY-PC stimulated emission, (327/517),
BoDIPY-PC fluorescence (509/517),
Fast-DiI stimulated emission (509/565),
Fast-DiI fluorescence (549/565),
Vesicle scattering (420/420).

Signal in the stimulated acceptor emission (SAE) channels contains non-FRET contributions from donor (D) and acceptor (A) emission through their direct excitation pathways, as well as excitation light scattered by the vesicle suspension. Control samples were used to correct for these contributions (see Document S1 in the Supporting Material).

FRET data analysis

Following Buboltz (14) and Smith and Freed (16), SAE in a two-dimensional tieline field is modeled by

$$F\left(u, S_{Lo}, \kappa^D, \kappa^A, \varphi\right)$$
$$= \frac{f_{Ld}(u,\varphi) + S_{Lo}[f_{Lo}(u,\varphi)K(u,\kappa^D)K(u,\kappa^A) - f_{Ld}(u,\varphi)]}{[1 + (K(u,\kappa^D) - 1)S_{Lo}][1 + (K(u,\kappa^A) - 1)S_{Lo}]},$$
$$(1)$$

$$K(u, \kappa) = 10^{\kappa_0 u + (\kappa_1 - \kappa_0)u^2}, \quad (2)$$

$$f(t, \varphi) = \varphi_0 + (\varphi_1, \varphi_2) \cdot B(t), \quad (3)$$

where u is the tieline coordinate, S_{Lo} is the Lo phase mole fraction, K are functions describing D and A partition coefficient variation within the tieline field, f_{Ld} and f_{Lo} are functions describing SAE variation in compositions along the phase boundaries, and $B(t)$ is the Ld + Lo boundary. Equations 2 and 3 were chosen to vary smoothly and allow a range of reasonable behaviors with a minimal number of fitting parameters (κ and φ). Data in the two-phase region were fit by optimizing κ^D, κ^A, and φ. Analysis was performed with Mathematica 7.0.1 (Wolfram Research, Champaign, IL). Full details are provided in Document S1 in the Supporting Material.

ESR sample preparation

Multilamellar vesicle samples were prepared by hydrating lipid films. Lipids and probe (16-PC) were dispensed into glass culture tubes with a Hamilton syringe. Samples contained ~2000 nmoles total lipid with 0.2 or 0.3 mol % 16-PC. Samples were dried to a thin film by rotary evaporation at ~60°C and placed under vacuum for 12–24 h to remove residual solvent. The dry film was hydrated at 60°C with 400 μL prewarmed RSE buffer, immediately followed by vortexing and five freeze/thaw cycles between liquid nitrogen and 60°C water. Samples were sealed under Ar and placed in a 60°C water bath, cooled at 2°C/h to ambient temperature, and incubated for >24 h. Before measurement, samples were pelleted and transferred to 1.5–1.8 × 100-mm glass capillaries.

ESR data analysis

Dynamic parameters for 16-PC in the slow-motional regime were obtained from nonlinear least-squares fits of simulations (17) based on the stochastic Liouville equation (18). Details of the analysis are found in Document S2 in the Supporting Material.

RESULTS

Regions of enhanced (reduced) FRET efficiency correspond to phase-coexistence regions

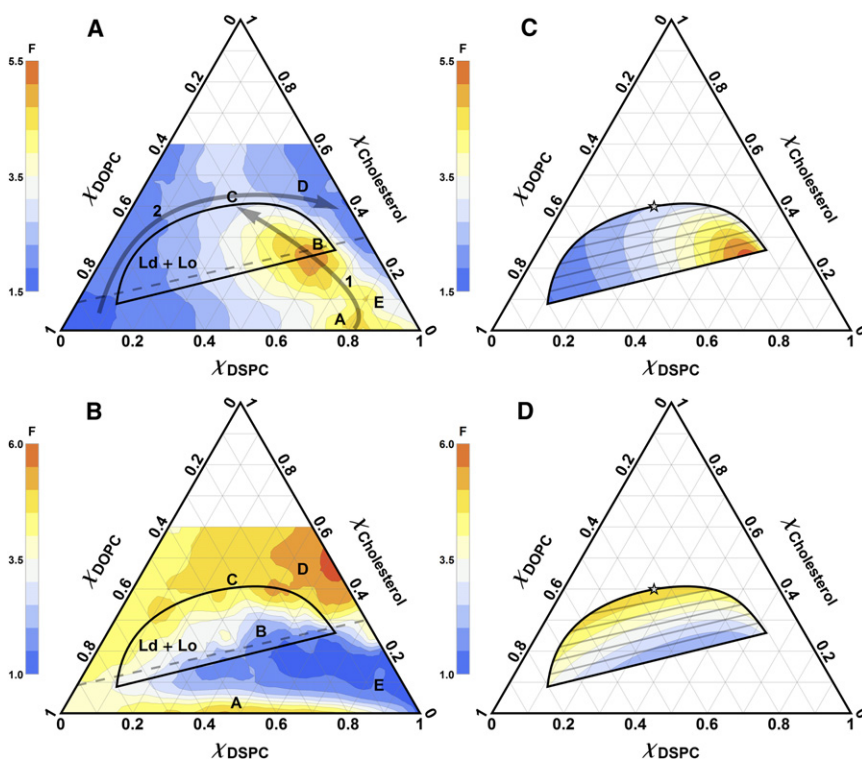Fig. S1.2 in the Supporting Material models a particularly useful FRET experiment for examining

FIGURE 1 SAE (stimulated acceptor emission) surfaces in DSPC/DOPC/chol show regions of enhanced or reduced FRET efficiency corresponding to phase coexistence regions. Contour plots *A* and *B* from 1116 data points, corresponding to 2 mol % sampling of the ternary composition space. Data were smoothed by averaging nearest-neighbor values. The relatively lowest values are blue, and the relatively highest values are red as shown by the scale bar. (*A*) BoDIPY-PC to Fast-DiI FRET: donor and acceptor colocalization in Ld phase domains results in enhanced FRET, most pronounced near the ordered phase boundary (*arrow* 1). (*B*) DHE to BoDIPY-PC FRET: donor and acceptor segregation between ordered and disordered phases results in reduced FRET. Symbols and arrows refer to surface features mentioned in the text. (*C* and *D*) Predicted surfaces for the Ld + Lo region corresponding to a best-fit of data in panels *A* and *B* (respectively) to Eqs. 1–3. Critical point (*star*) and tieline field used to model the data are shown.

composition-dependent phase behavior in lipid bilayers: a set of samples is prepared along a tieline, with each sample receiving a fixed amount of D and A probe. Shown is the family of FRET curves generated by Eq. S1.3 as K^A varies with fixed K^D, revealing two general lineshapes. When D and A prefer the same phase, FRET increases abruptly at the phase boundary where the favored phase first appears. Relative to a straight line joining the endpoint values, FRET is enhanced at all phase-separated compositions. When D and A prefer different phases, the opposite effect is seen: FRET decreases abruptly at each phase boundary and is reduced at all compositions along the tieline. These two characteristic lineshapes are termed, respectively, region of enhanced efficiency (REE) and region of reduced efficiency (RRE). Although FRET varies with composition even in the absence of phase coexistence, changes within a single phase are expected to be gradual and small relative to those induced by phase separation.

Analogous to the one-dimensional tieline, the FRET surface for a two-dimensional tieline field with smoothly varying K^P, described by Eqs. 1–3, exhibits a characteristic three-dimensional peak of enhanced efficiency if D and A colocalize, and a three-dimensional valley of reduced efficiency if D and A separate in the coexistence region. We chose two FRET pairs to generate both behaviors: a cholesterol analog (DHE) that partitions into Lo phase, paired with the Ld-preferring probe BoDIPY-PC; and BoDIPY-PC paired with a second Ld-preferring probe, Fast-DiI. Consistent with expectations, clear and interpretable patterns are

observed: FRET between DHE (D) and BoDIPY-PC (A) is reduced in DSPC/DOPC/chol phase-coexistence regions relative to the surrounding single-phase regions (see Fig. 1 B), while FRET between BoDIPY-PC (D) and Fast-DiI (A) is enhanced (see Fig. 1 A). We now describe key features of these surfaces.

FRET surfaces in DSPC/DOPC/chol

BoDIPY-PC to Fast-DiI: enhanced FRET

Both probes prefer Ld phase, yielding REE peaks in compositional regions where Ld coexists with an ordered phase, and is the minor component. We note these qualitative features of the FRET surface in Fig. 1 A:

1. A ridge of enhanced FRET (*gray curved arrow* 1). Most of the composition space below $\chi_{CHOL} = 0.4$ separates into coexisting Ld and ordered phase (Lo, Lβ, or both). Tielines have small positive slope, indicating slightly increased concentration of cholesterol, up to ~2.5-fold, in Lo. The ridge of enhanced FRET results from increased concentration of D and A in the diminishing Ld phase, and concomitant decrease in average D-A separation.

2. The upper boundary of the liquid/liquid region at χ_{CHOL} ~0.4, manifests as a sharp increase in FRET (e.g., from point D to B).

3. The relative magnitude of FRET in the gel/liquid and liquid/liquid regions differs, with the REE peak in the

TABLE 1   Best-fit parameter values with standard deviations for FRET data in the Ld + Lo region of DSPC/DOPC/chol, modeled by Eqs. 2 and 3

κ_0^{DHE}	κ_1^{DHE}	κ_0^{BoDIPY}	κ_1^{BoDIPY}	κ_0^{Dil}	κ_1^{Dil}	φ_0^{RRE}	φ_1^{RRE}	φ_2^{RRE}	φ_0^{REE}	φ_1^{REE}	φ_2^{REE}
0.45(0.1)	0.1(0.4)	−1.0(0.2)	−1.0(0.6)	−0.8(0.2)	−1.0(0.6)	3.3(0.4)	−2(1)	8(3)	1.51(0.04)	1.5(0.3)	1.5(0.3)

latter (point *B*) ~15% greater than in the former (point *A*). This difference in FRET intensity could result from the geometry and small size of gel/liquid phase domains at high χ_{DSPC}.

4. FRET efficiency is enhanced in single-phase compositions near the critical point. The path through composition space (marked by *gray curved arrow* 2) follows a continuous phase change from Ld to Lo; a modest rise and fall in FRET intensity occurs in the single phase vicinity of the critical point (point *C*). Thus, even in the absence of a sharp transition, molecular interactions giving rise to Ld and Lo coexistence at lower χ_{CHOL} cause compositional fluctuations sensed by the probes in this single-phase region.

5. Along the DOPC/chol binary axis, modest changes in FRET are consistent with complete miscibility.

6. Along the binary DSPC/chol axis, FRET decreases from a high value at the DSPC vertex to a low value near $\chi_{CHOL} = 0.27$, then remains nearly constant up to high χ_{CHOL}. The gradual change in FRET is consistent with the absence of any first-order phase transition along this axis (19).

DHE to BoDIPY-PC: reduced FRET

Like cholesterol, DHE partitions modestly into ordered phases. The FRET surface between DHE and BoDIPY-PC in the Lβ + Lo and Ld + Lo regions is dominated by valleys of reduced efficiency due to probe separation (Fig. 1 *B*, regions near points *E* and *B*). We further note the following:

1. The upper Ld + Lo boundary is seen as an abrupt decrease in FRET efficiency upon entering the two-phase region (e.g., from point *D* to *B*).

2. FRET in the Ld + Lβ region at low cholesterol (region near point *A*) is modestly enhanced relative to single-phase Ld, suggesting that DHE (or cholesterol) prefers Ld over Lβ'. The same result was found for DHE in DPPC (1,2-dipalmitoyl-*sn*-glycero-3-phosphocholine)/ DLPC (1,2-dilauroyl-*sn*-glycero-3-phosphocholine) at 20°C and DPPC/DOPC at 25°C (14,20), and likely reflects an energetic penalty for creating defects in a tilted Lβ' lattice. When cholesterol is added to DSPC/DOPC mixtures (e.g., from point *A* to *B*), a decrease in FRET occurs as DHE preference shifts from Ld to Lβ. The change in DHE partitioning might relate to the transformation of the gel from a tilted Lβ' to an untilted Lβ phase that more easily accommodates sterols (19).

3. Modest changes in FRET along the DOPC/chol binary axis are consistent with uniform mixing.

Probe partitioning in DSPC/DOPC/chol

FRET data in the Ld + Lo region were modeled with Eqs. 1–3 to recover probe K^P, using a fixed tieline field. The phase boundary was taken from Zhao et al. (6) with slight modification. The critical point and tieline slopes were constrained with phase percolation data and direct observation of critical fluctuations in GUVs (see Fig. S1.5 and Fig. S1.6). Best-fit surfaces are shown in Fig. 1, *C* and *D*, and the recovered parameters are listed in Table 1.

Equation 2 describes probe partitioning between coexisting phases: for a particular tieline (i.e., a particular value of *u*), the best-fit parameters κ_0 and κ_1 give the partition coefficient K^P. Fig. 2 plots K^P for DHE, BoDIPY-PC, and Fast-DiI using their respective best-fit values of κ_0 and κ_1 found in Table 1, across the Ld + Lo tieline field. For comparison, K^P of lipid components calculated from tieline endpoint compositions are also shown in Fig. 2. The structural analogs DHE and cholesterol partition similarly to each other, weakly favoring the Lo phase. Both BoDIPY-PC and Fast-DiI strongly prefer the Ld phase; like DOPC, these probes have structural motifs that disrupt ordered lipid lattices.
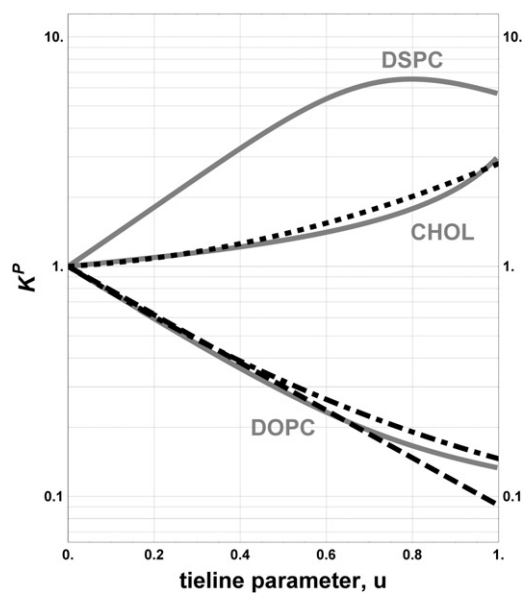

FIGURE 2   Lipid and probe K^P in the Ld + Lo tieline field of DSPC/DOPC/chol. Each value of *u* represents a different tieline, beginning at the critical point (*u* = 0) and ending at the Ld + Lo segment of the three-phase triangle (*u* = 1). DHE (*dotted*), BoDIPY-PC (*dashed*), and Fast-DiI (*dot-dash*) K^P are calculated from Eq. 2 and the respective best-fit values of κ_0 and κ_1 listed in Table 1. Lipid K^P (*shaded lines*) are calculated from tieline endpoints.

FRET surfaces in DSPC/POPC/chol and DSPC/SOPC/chol

FRET was examined for DSPC/POPC/chol and DSPC/SOPC/chol under sample preparation and measurement conditions essentially identical to those used for DSPC/DOPC/chol. As with DSPC/DOPC/chol, these mixtures exhibit coexisting gel/liquid at low cholesterol concentration when GUVs are examined with fluorescence microscopy (9). Unlike DSPC/DOPC/chol, GUVs with compositions above the gel/liquid region appear uniform under the microscope. Nevertheless, FRET features, shown in the last section to arise from probe-partitioning and the lever rule, exist above the gel/liquid region in these systems as described below.

BoDIPY-PC to Fast-DiI

1. A ridge of enhanced FRET is marked by gray curved arrow 1 in Fig. 3, A and B, analogous to arrow 1 in Fig. 1 A. A peak of enhanced FRET in DSPC/POPC/chol (point B) corresponds to point B in the Ld + Lo region of DSPC/DOPC/chol (see Fig. 1 A), the result of probe colocalization in Ld domains. In contrast, the ridge in DSPC/SOPC/chol (see Fig. 3 B, arrow 1) contains no local peak near B, but instead runs continuously into the larger REE peak of the gel/liquid region (point A). The relative FRET enhancement in the Ld + Lo region of these systems is smaller than for the DOPC-containing system, indicating that phase domains are comparable in size to R_0. The absence of a FRET peak at point B in DSPC/SOPC/chol might indicate a further reduction in domain size in the SOPC system compared with the POPC system.

2. The upper Ld + Lo boundary is marked by an increase in FRET efficiency upon entering the two-phase region, shown clearly on the path between points D and B.

DHE to BoDIPY-PC

1. The upper Ld + Lo boundary shows up in a similar way in all three mixtures. There is a remarkable similarity of Fig. 3, C and D to Fig. 1 B: A phase boundary appears as a relatively abrupt change in FRET at χ_{CHOL} ~0.30 (e.g., between points D and B in Fig. 3, C and D). This upper boundary extends from the binary DSPC/chol axis to at least $\chi_{DSPC} = 0.2$ and therefore must include parts of both the Lo + Lβ and Ld + Lo boundaries. It is clearly distinct from the upper boundary of macroscopic gel/liquid coexistence observed in GUV experiments, which does not extend above $\chi_{CHOL} = 0.18$ in either system (9).

2. FRET efficiency in Ld + Lo is reduced relative to that in the surrounding one-phase regions, but to a lesser extent than in the DOPC-containing mixture. This effect is expected when phase domain size is comparable to R_0.

Summary of FRET surfaces for the three mixtures

1. Overall FRET patterns, both RRE and REE, are the same for the three mixtures, reflecting similarity of their phase behavior over all composition space.
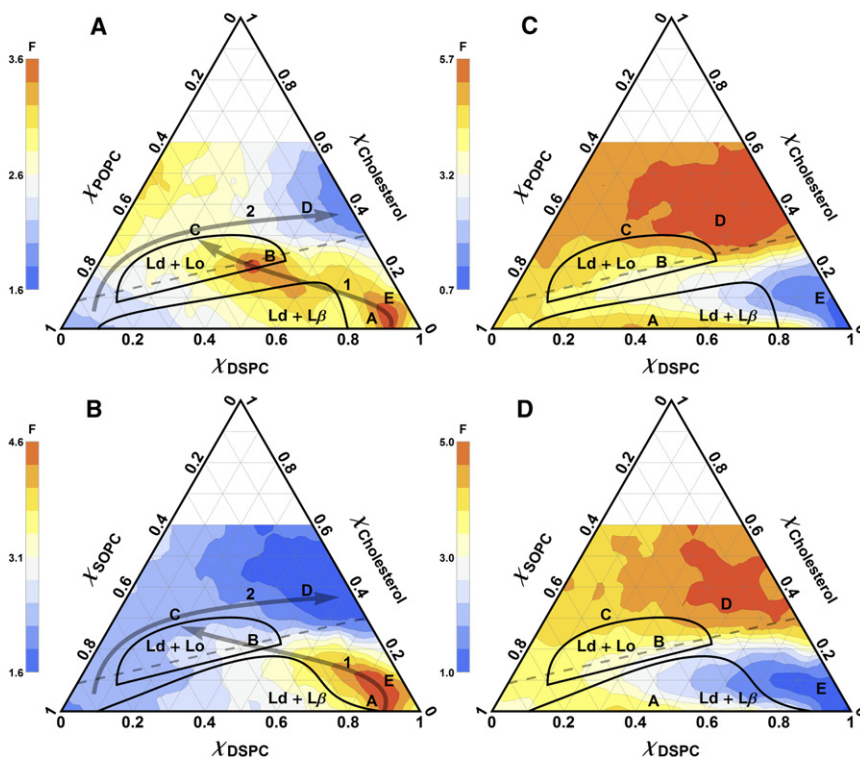

FIGURE 3 SAE surfaces in DSPC/POPC/chol and DSPC/SOPC chol show RRE and REE. Contour plots A and B each from 1116 data points, corresponding to 2% sampling of the ternary composition space. Data were smoothed by averaging nearest-neighbor values. BoDIPY-PC to Fast-DiI FRET in DSPC/POPC/chol (A) and DSPC/SOPC/chol (B). As in Fig. 1, colocalization of these probes in Ld phase domains results in enhanced FRET efficiency at phase-separated compositions. DHE to BoDIPY-PC FRET in DSPC/POPC/chol (C) and DSPC/SOPC/chol (D). Separation of these probes between ordered and disordered phases results in reduced FRET efficiency. Symbols and arrows refer to surface features mentioned in the text.

2. Cholesterol interacts more favorably with POPC and SOPC than with DOPC. 40 mol % cholesterol must be added to DSPC/DOPC mixtures to achieve miscibility, compared to 30 mol % for DSPC/POPC or DSPC/SOPC.

3. The magnitudes of FRET variations across all compositions are greatest in the DOPC-containing mixtures: the maximum FRET enhancement in the Ld + Lo region is greatest in DSPC/DOPC/chol, smaller when DOPC is replaced by POPC, and smaller still with replacement by SOPC. These changes can be explained by a reduction in probe K^P, a reduction in phase domain size, or both.

ESR spectroscopy

Fig. S1 shows interpolated FRET data along an Ld + Lo tie-line near the three phase region, corresponding to the dashed lines in Figs. 1 and 3. The patterns of enhanced and reduced FRET efficiency predicted by Eq. S1.3 are apparent, although precise phase boundaries are in some cases difficult to determine. ESR was used to further examine the physical properties of mixtures along this sample trajectory. Experimental spectra were simulated to extract order and dynamic parameters. Plots of typical spectra are shown in Fig. S2.1, and a discussion of simulation parameters is found in Document S2 in the Supporting Material.

Fig. 4 A shows the order parameter S_0 for 16-PC as a function of mixture composition, assuming a single environment for the probe. For samples near the binary DSPC/chol axis, $S_0 \sim 0.25$, typical of 16-PC in an Lo phase (21). Chain order decreases as low-T_M lipid is incorporated into the bilayer and eventually falls to values ($S_0 \sim 0.05$) typical of 16-PC in an Ld phase. A sharp drop in S_0 occurs in each ternary mixture, consistent with redistribution of 16-PC between coexisting phase environments. Though the recovered value of S_0 represents an average of values in the coexisting phases, it does not simply reflect the relative amounts of the two phases present. Because the first-derivative signal varies inversely with the square of the resonance linewidth (see Fig. S2.1), we speculate that the narrow disordered component is dominating the fit.

To quantify the distribution of 16-PC between Ld and Lo, we modeled each spectrum as a weighted superposition of Ld- and Lo-like spectra, using the binary-axis (endpoint) compositions as basis spectra. The best-fit weights (w_{Lo}, w_{Ld}) directly yield the fraction of 16-PC in the Lo phase:

$$f_{16PC}^{Lo} = \frac{w_{Lo}}{w_{Lo} + w_{Ld}}. \tag{4}$$

Fig. 4 B plots the 16-PC fraction in the Lo phase determined at each composition using Eq. 4. Assuming the sample trajectory is collinear with a tieline and the probe does not partition preferentially to the interface between domains, the probe fraction in the Lo phase can be expressed as a function of the phase boundaries (χ^{Ld}, χ^{Lo}) and the K^P of 16-PC:
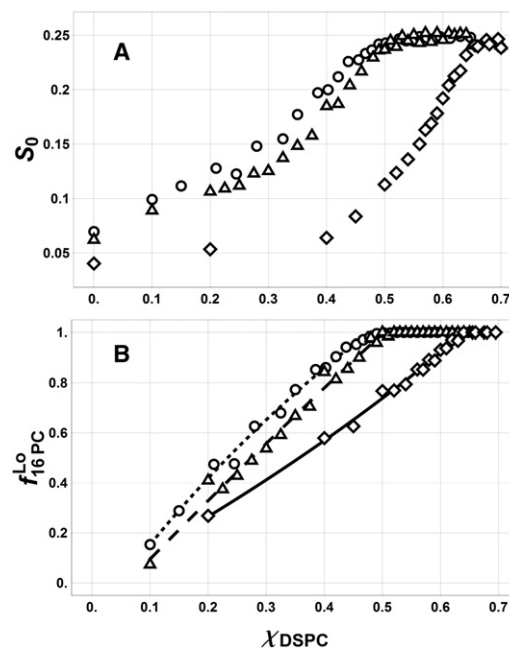

FIGURE 4   ESR reveals similarities in phase properties of mixtures forming macroscopic and nanoscopic phases. Compositional trajectories run in the approximate direction of Ld + Lo tielines (see Fig. 1 A, *dashed line*) and differ only in the identity of the low-T_M lipid. (*A*) Composition-dependent order parameters obtained from ESR spectral simulations in DSPC/DOPC/chol (*diamonds*), DSPC/POPC/chol (*triangles*), and DSPC/SOPC/chol (*circles*). (*B*) Fraction of 16-PC spin probe in the Lo phase determined by spectral subtraction using Eq. 4 (*symbols* as in panel A). Predicted fractions from Eq. 5 shown as lines for DSPC/DOPC/chol (*solid*), DSPC/POPC/chol (*dashed*), and DSPC/SOPC/chol (*dotted*), with best-fit parameters listed in Table 2.

$$f_{16PC}^{Lo}\left(\chi; \chi^{Ld}, \chi^{Lo}, K^{16PC}\right)$$
$$= \begin{cases} 0 & \chi \leq \chi^{Ld} \\ \dfrac{K^{16PC}}{K^{16PC} + \dfrac{\chi^{Lo} - \chi}{\chi - \chi^{Ld}}} & \chi^{Ld} < \chi < \chi^{Lo} \\ 1 & \chi \geq \chi_{Lo} \end{cases} \tag{5}$$

Both phase boundaries and K^{16PC} were varied in the fit. Model predictions are shown as lines in Fig. 4 B, with recovered parameters listed in Table 2. 16-PC partition between Ld and Lo is close to unity, similar to values seen for coexisting gel/liquid of DPPC/DLPC/chol (22). The recovered Lo phase boundaries coincide with the abrupt drop in S_0 shown in Fig. 4 A. The recovered Ld phase boundary for DSPC/DOPC/chol is considerably lower in DSPC than values determined by FRET and confocal fluorescence microscopy, most likely due to the paucity of data points near this boundary.

The location of the phase boundary at high χ_{DSPC} reveals quantitative differences in molecular interactions: the Lo phase accommodates significantly more monounsaturated

TABLE 2 Best-fit phase boundaries and 16-PC partition coefficients with standard deviations, modeled by Eq. 5

System	χ_{DSPC}^{Ld}	χ_{DSPC}^{Lo}	K^{16PC}
DSPC/DOPC/chol	0(0.02)	0.64(0.003)	0.80(0.06)
DSPC/POPC/chol	0.06(0.01)	0.50(0.005)	1.05(0.08)
DSPC/SOPC/chol	0.05(0.01)	0.48(0.005)	1.3(0.1)

lipid, evidence of a more favorable interaction with DSPC for these lipids compared to DOPC. Only 8 mol % DOPC is required to precipitate an Ld phase along this trajectory. In contrast, ~25 mol % POPC or SOPC is required for phase separation. Up to the point of phase separation, the Lo phase maintains a nearly constant order parameter of 0.25 and diffusion coefficient of 9×10^7 s^{-1} (data not shown), indicating only minor changes in bilayer properties as a function of composition within the Lo region.

Physical properties of the Ld phase exhibit greater dependence on lipid structure, apparent in Fig. 4 A. The Ld phase at low DSPC becomes progressively ordered in the series DOPC < POPC < SOPC. For compositions on the binary axis consisting of the low-T_M lipid with $\chi_{CHOL} = 0.09$, S_0 increases 75% upon saturation of the sn-1 chain (equivalent to replacing DOPC with SOPC). In contrast, shortening the sn-1 chain by two carbons (i.e., replacing SOPC with POPC) increases fluidity, evidenced by a 10% decrease in S_0. This trend continues with addition of DSPC and persists until the disappearance of Ld phase, at which point S_0 is the same for the three mixtures. Fig. 4 B shows that these differences in order are also reflected in 16-PC partitioning between Ld and Lo. Because ΔS_0 between the coexisting environments decreases in the series DOPC > POPC > SOPC, there is less tendency for the bulky spin probe to be driven out of the ordered phase, and the 16-PC concentration in Lo increases.

DISCUSSION

Motivation and experimental design

Systems studied here are simple models for the mammalian plasma membrane outer leaflet: ternary mixtures containing cholesterol and the high-T_M lipid DSPC, with a series of three low-T_M lipids DOPC, POPC, and SOPC. Despite the structural similarity of the low-T_M lipids, exchanging DOPC for either POPC or SOPC results in dramatically different mixing behavior at biologically relevant cholesterol concentrations (10–40 mol %), as revealed by fluorescence microscopy of GUVs. The micron-sized liquid phase domains in DSPC/DOPC/chol are not observed at any composition in DSPC/SOPC/chol or DSPC/POPC/chol (4,9). POPC is an important lipid for model studies due to its biological abundance and has been chosen as the representative low-T_M lipid in several recent studies of ternary mixtures (7,8,11). Each of these studies used a sphingomyelin (SM) as the high-T_M lipid, employed methods sensitive to small length scales, and reported a region of Ld + Lo phase coexistence.

In contrast, a FRET study comparing DPPC/DOPC/chol with DPPC/POPC/chol reported Ld + Lo coexistence in the former system, but not in the latter (23). Together, these studies reveal that even small structural differences in both the high- and low-T_M components can dramatically affect phase coexistence and/or domain size. We add to these reports a comparison of three ternary mixtures at high-compositional resolution using methods that are sensitive to small (>2 nm) heterogeneities.

The high throughput of our RSE sample preparation technique enabled us to evenly sample the ternary composition space at 2% resolution. For each mixture, we examined ~1100 samples and several hundred control samples. We previously discovered that systematic errors occur in large data sets when samples are prepared and measured in a well-defined order (e.g., low to high DSPC, or low to high cholesterol), due primarily to a small, gradual change in the concentration of chloroform solutions of lipid and probe. In this study, data were collected and measured in random order to minimize any systematic distortion of surface features. The trade-off inherent in this approach is a greater overall noise level. FRET surfaces are consequently less useful for establishing precise phase boundaries than targeted, smaller-scale experiments (i.e., short linear sample trajectories that cross a phase boundary). Their value lies in establishing the overall pattern of phase behavior of a mixture.

Comparison of phase behavior in three ternary systems

Our basis mixture for investigating influence of the low-T_M lipid on liquid domain size is DSPC/DOPC/chol. We begin with a discussion of phase behavior in this system. The complete phase diagram for DSPC/DOPC/chol is shown in Fig. 5. For illustrative purposes, we consider the phase behavior of a hypothetical sample with equal mole fractions
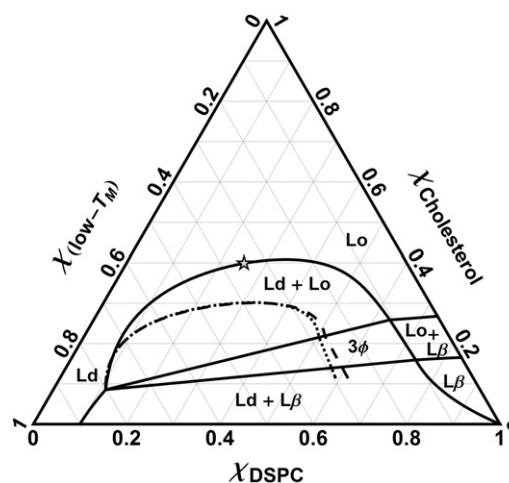

FIGURE 5 Phase diagrams for systems in this study: DSPC/DOPC/chol (solid lines), DSPC/POPC/chol (dashed), and DSPC/SOPC/chol (dotted). Solidus boundary extensions are not well determined in the POPC- and SOPC-containing mixtures.

of DOPC and DSPC and continuously increasing cholesterol concentration. In the absence of cholesterol, DOPC is practically insoluble in the pure DSPC gel (Lβ'), and the sample is composed of roughly equal mole fractions of Ld and Lβ' phase with compositions $\chi_{DSPC} = 0.1$ and 1, respectively (6). As cholesterol is added, its distribution between the coexisting phases initially favors Ld, as evidenced by enhanced FRET between DHE and the Ld-preferring BoDIPY-PC at low χ_{CHOL} (see Fig. 1 B). Upon further addition of cholesterol, DSPC chain tilt is abolished, and both cholesterol and DOPC solubility increase in the gel phase (now Lβ).

As cholesterol distribution shifts to favor the Lβ phase, FRET efficiency between DHE and BoDIPY-PC decreases. Cholesterol eventually reaches a saturating concentration of $\chi_{CHOL} \sim 0.16$ in the Lβ phase and a third, Lo phase with higher cholesterol content forms. Along this 1:1 DSPC/DOPC trajectory, the three phases coexist over a small composition range, with Lo effectively replacing Lβ as cholesterol concentration increases from 12 to 18 mol % (the fraction of Ld phase is roughly constant along this path). Further addition of cholesterol beyond $\chi_{CHOL} \sim 0.18$ has a differential effect on chain order in the coexisting phases, as seen in the ESR trajectories. Order increases in the Ld phase as DOPC chains are forced into a smaller cross-sectional area to shield cholesterol from contact with water in the headgroup region, while order in the Lo phase is essentially unchanged. Eventually the difference in chain order is too small to sustain phase separation: above $\chi_{CHOL} = 0.4$, the bilayer exists as a single phase with small compositional fluctuations.

Upon replacing DOPC with either POPC or SOPC, the same phase coexistence regions are observed with FRET, but phase boundaries have shifted in a manner consistent with increased acyl chain order in POPC- or SOPC-rich Ld phases (see Fig. 5). POPC and SOPC are significantly more soluble in the Lβ and Lo phases than is DOPC, composing >25 mol % of these phases at maximum solubility, before precipitation of the Ld phase. However, as in the DOPC-containing mixtures, cholesterol is soluble in gel up to $\chi_{CHOL} \sim 0.16$. Both POPC and SOPC mixtures are more ordered than DOPC mixtures at all cholesterol concentrations. Consequently, Ld + Lo phase separation is abolished at lower cholesterol concentrations, with FRET data indicating an upper phase boundary at $\chi_{CHOL} \sim 0.3$.

Quantitative analysis of dye partitioning in DSPC/DOPC/chol (see Fig. 2) confirms that the fluorescent sterol DHE is a faithful reporter of cholesterol distribution (24). Similarly, the distribution of BoDIPY-PC and Fast-DiI between Ld and Lo reflects the distribution of DOPC between these phases. Maximum partitioning occurs at the three-phase triangle just before precipitation of the Lβ phase, where physical differences (e.g., order) between Ld and Lo phases are greatest. Consequently, the FRET peak between BoDIPY-PC and Fast-DiI is located on this tieline (see Fig. 1 A). The central

FRET peak in DSPC/POPC/chol (see Fig. 3 A, point B) similarly must be located at a composition very near the Ld + Lo leg of the three-phase triangle. Furthermore, GUV and FRET data (not shown) narrowly constrain the location of the Ld vertex of the three-phase triangle, and together these two points define the approximate direction of the first Ld + Lo tieline.

Comparison of DSPC/POPC/chol with other POPC-containing ternary systems

Phosphatidylcholines are among the most abundant lipids in mammalian PM. Approximately 50 mol % of the outer leaflet lipid is PC, with POPC and SOPC typically being the predominant species (25). Because of its biological relevance, POPC was used as the low-T_M lipid in much of the pioneering work on ternary phase behavior. Our study invites comparison with these systems, particularly those studied using techniques sensitive to nanometer-scale heterogeneities.

de Almeida et al. (7) used fluorescence anisotropy and lifetime-weighted quantum yield to obtain a phase diagram for palmitoyl-SM/POPC/chol. Halling et al. (11) reported similar results with the same lipid system and experimental techniques, though they also employed probes sensitive to the onset of gel phase and thereby recorded the Ld + Lo segment of the three-phase triangle to greater precision. Both groups reported similar phase behavior at 23°C: three two-phase binary systems extending into the ternary composition space and joined by a three-phase region. Pokorny et al. (8) published a similar phase diagram for brain-SM/POPC/chol, with the notable difference that the Ld + Lo region terminated in a critical point near the binary POPC/chol axis.

The reported phase behavior for the POPC/chol axis (where the diagrams are directly comparable) deserves further comment. de Almeida et al. (7) and Halling et al. (11) show a region of Ld + Lo coexistence between $\chi_{CHOL} = 0.12-0.44$, whereas Pokorny et al. (8), in agreement with our study, shows complete miscibility of the components to at least $\chi_{CHOL} = 0.4$. This discrepancy has important consequences for the estimated uncertainty of a proposed tieline in de Almeida et al. (7), as their analysis relied on the limiting tieline slopes at the three-phase triangle and binary POPC/chol axis. Spatial sensitivity of the experiments is the most likely explanation for conflicting results. SP-FRET detects changes in D and A spatial distributions on length scales greater than a few times R_0, and formation of lipid clusters smaller than a few nanometers cannot be observed above the baseline FRET signal of a random probe distribution.

In contrast, fluorescence anisotropy and quantum yield are sensitive to the immediate environment of the fluorescent molecule: composition differences in the nearest-neighbor shell surrounding a probe can yield distinct signals, and hence small clusters of lipids can appear as

distinct nanoenvironments even for ordinary nonideal mixing. An important distinction must be drawn between coexisting phase domains and these very local compositional fluctuations that are present in any nonideal mixture, as only the former are constrained by the Lever rule for first-order phase separation. FRET is therefore an important tool for distinguishing these cases: the sixth-power distance dependence effectively acts as a spatial filter by averaging out the effects of short-range compositional fluctuations.

Limitations of SP-FRET for establishing phase behavior

As noted in the previous section, diminished sensitivity of SP-FRET to the smallest domains (i.e., those comparable in size to R_0) may limit its usefulness in establishing phase coexistence in some mixtures. Variation in the domain size distribution within a phase coexistence region can confound the precise determination of phase boundaries, particularly if parts of the phase-coexistence region near one or both phase boundaries exhibit small domains: the apparent coexistence region would be smaller than the true coexistence region.

In the extreme case that an entire coexistence region exhibits domains smaller than R_0, it might be indistinguishable from surrounding one-phase regions in the SP-FRET surface; the probability of this artifact is minimized by using probes with small R_0 (14). The D/A pairs used in this study have R_0 of ~2.5 nm (DHE/BoDIPY-PC) and 6.5 nm (BoDIPY-PC/Fast-DiI) as calculated from spectral overlap integrals. The close correspondence of SP-FRET surface features of the two probe pairs (particularly in the Ld + Lo region) suggests that liquid domain sizes are no smaller than ~5 nm in the mixtures studied.

Phaselike behavior of nanodomains

It is becoming increasingly clear that suboptical lateral organization is a general phenomenon that occurs in many binary and ternary mixtures (26,27). However, considerable debate continues as to whether nanoscopic domains constitute first-order phase separation. Line tension at domain boundaries always favors coalescence of small domains into a single large domain at equilibrium. Thermodynamic stability of small domains thus would require small line tension together with a free energy contribution opposing domain coalescence. Line tension is reduced by the presence of line-active molecules, a role that has been suggested for cholesterol (28,29), asymmetric saturated/monounsaturated lipids like POPC and SOPC (30), and fluorescent impurities (31).

Theoretical work has related line tension to hydrophobic mismatch at domain boundaries (32), and a recent AFM/fluorescence microscopy study demonstrated that a decreasing height mismatch between Ld and Lo domains resulted in stable arrays of increasingly smaller domains (33). In GUV systems containing POPC, cholesterol, and a saturated PC of varying length, liquid domains were not observed at 1:1:1 composition for DPPC and DSPC (with 16- and 18-carbon chains, respectively), but were visible with 20-carbon 1,2-diarachidoyl-*sn*-glycero-3-phosphocholine (4).

Further exploration is needed to understand the molecular origin of line tension and its dependence on lipid composition and temperature. Ultimately, no special mechanism is required to explain vanishingly small line tensions in phase-separated mixtures, as line tension must approach zero near a critical point. This has been demonstrated experimentally in ternary systems both by varying temperature at a fixed composition toward an upper miscibility critical point (34) and by varying composition at fixed temperature toward a consolute point (35).

Even though small line tensions are expected and observed in phase-separated compositions near critical points, the thermodynamic stability of small phase domains requires a competing energy term favoring dispersed domains. For unsupported bilayers like those studied here, curvature has been proposed to compete with line tension (13,36). Another possibility is that within the Lo phase, the competition of individual cholesterol molecules for solvating PC neighbors is frustrated as the phase domain grows (37). Much work remains to explain the stability of small domains.

CONCLUSIONS

We previously reported the absence of visible liquid domains in DSPC/POPC/chol and DSPC/SOPC/chol (9). Using methods with submicron sensitivity, we have found that, in fact, these mixtures exhibit similar phase behavior to DSPC/DOPC/chol, including liquid phase coexistence. We have shown that FRET and ESR data in DSPC/POPC/chol and DSPC/SOPC/chol are consistent with first-order phase transitions: changes in signal with composition are consistent with phase boundaries and the lever rule.

Our data also suggest the location of an Ld + Lo tieline in DSPC/POPC/chol. As an experimental system, this tieline offers several advantages to the study of raft properties: the compositions of coexisting phases are well defined, the phase fractions are constrained by the Lever rule, and the domain sizes are comparable to those suggested for biological rafts.

We expect that further study of this tieline will provide more realistic data for lipid and protein partitioning between raftlike Ld and Lo domains, and valuable insight into the physical mechanisms that limit domain size in biological membranes.

SUPPORTING MATERIAL

Two additional sections with twelve figures, four tables, and 32 equations are available at http://www.biophysj.org/biophysj/supplemental/S0006-3495 (10)01215-4.

REFERENCES

1. Lingwood, D., and K. Simons. 2010. Lipid rafts as a membrane-organizing principle. *Science.* 327:46–50.

2. Kusumi, A., and K. Suzuki. 2005. Toward understanding the dynamics of membrane-raft-based molecular interactions. *Biochim. Biophys. Acta.* 1746:234–251.

3. Elson, E. L., E. Fried, …, G. M. Genin. 2010. Phase separation in biological membranes: integration of theory and experiment. *Annu. Rev. Biophys.* 39:207–226.

4. Veatch, S. L., and S. L. Keller. 2003. Separation of liquid phases in giant vesicles of ternary mixtures of phospholipids and cholesterol. *Biophys. J.* 85:3074–3083.

5. Veatch, S. L., K. Gawrisch, and S. L. Keller. 2006. Closed-loop miscibility gap and quantitative tie-lines in ternary membranes containing diphytanoyl PC. *Biophys. J.* 90:4428–4436.

6. Zhao, J., J. Wu, …, G. W. Feigenson. 2007. Phase studies of model biomembranes: complex behavior of DSPC/DOPC/cholesterol. *Biochim. Biophys. Acta.* 1768:2764–2776.

7. de Almeida, R. F., A. Fedorov, and M. Prieto. 2003. Sphingomyelin/phosphatidylcholine/cholesterol phase diagram: boundaries and composition of lipid rafts. *Biophys. J.* 85:2406–2416.

8. Pokorny, A., L. E. Yandek, …, P. F. Almeida. 2006. Temperature and composition dependence of the interaction of δ-lysin with ternary mixtures of sphingomyelin/cholesterol/POPC. *Biophys. J.* 91:2184–2197.

9. Zhao, J., J. Wu, …, G. Feigenson. 2007. Phase studies of model biomembranes: macroscopic coexistence of Lα+Lβ, with light-induced coexistence of Lα+Lo Phases. *Biochim. Biophys. Acta.* 1768:2777–2786.

10. Silvius, J. R. 2003. Fluorescence energy transfer reveals microdomain formation at physiological temperatures in lipid mixtures modeling the outer leaflet of the plasma membrane. *Biophys. J.* 85:1034–1045.

11. Halling, K. K., B. Ramstedt, …, T. K. Nyholm. 2008. Cholesterol interactions with fluid-phase phospholipids: effect on the lateral organization of the bilayer. *Biophys. J.* 95:3861–3871.

12. Dean, D. S., and M. Manghi. 2006. Fluctuation-induced interactions between domains in membranes. *Phys. Rev. E.* 74:021916.

13. Semrau, S., T. Idema, …, C. Storm. 2009. Membrane-mediated interactions measured using membrane domains. *Biophys. J.* 96:4906–4915.

14. Buboltz, J. T. 2007. Steady-state probe-partitioning fluorescence resonance energy transfer: a simple and robust tool for the study of membrane phase behavior. *Phys. Rev. E.* 76:021903–021907.

15. Buboltz, J. T., and G. W. Feigenson. 1999. A novel strategy for the preparation of liposomes: rapid solvent exchange. *Biochim. Biophys. Acta.* 1417:232–245.

16. Smith, A. K., and J. H. Freed. 2009. Determination of tie-line fields for coexisting lipid phases: an ESR study. *J. Phys. Chem. B.* 113:3957–3971.

17. Budil, D. E., S. Lee, …, J. H. Freed. 1996. Nonlinear-least-squares analysis of slow-motion EPR spectra in one and two dimensions using a modified Levenberg-Marquardt algorithm. *J. Magn. Reson. A.* 120:155–189.

18. Schneider, D. J., and J. H. Freed. 1989. Calculating slow motional magnetic resonance spectra. A user's guide. *In* Spin Labeling: Theory and Application. J. Reuben, editor. Plenum, New York. 1–76.

19. Mills, T. T., J. Huang, …, J. F. Nagle. 2009. Effects of cholesterol and unsaturated DOPC lipid on chain packing of saturated gel-phase DPPC bilayers. *Gen. Physiol. Biophys.* 28:126–139.

20. Buboltz, J. T., C. Bwalya, …, M. Schutzer. 2007. High-resolution mapping of phase behavior in a ternary lipid mixture: do lipid-raft phase boundaries depend on the sample preparation procedure? *Langmuir.* 23:11968–11971.

21. Chiang, Y. W., Y. Shimoyama, …, J. H. Freed. 2004. Dynamic molecular structure of DPPC-DLPC-cholesterol ternary lipid system by spin-label electron spin resonance. *Biophys. J.* 87:2483–2496.

22. Chiang, Y. W., J. Zhao, …, G. W. Feigenson. 2005. New method for determining tie-lines in coexisting membrane phases using spin-label ESR. *Biochim. Biophys. Acta.* 1668:99–105.

23. Brown, A. C., K. B. Towles, and S. P. Wrenn. 2007. Measuring raft size as a function of membrane composition in PC-based systems: part II—ternary systems. *Langmuir.* 23:11188–11196.

24. Wüstner, D. 2007. Fluorescent sterols as tools in membrane biophysics and cell biology. *Chem. Phys. Lipids.* 146:1–25.

25. Gennis, R. B. 1989. Biomembranes: Molecular Structure and Function. C. R. Cantor, editor. Springer-Verlag, New York.

26. Marsh, D. 2009. Cholesterol-induced fluid membrane domains: a compendium of lipid-raft ternary phase diagrams. *Biochim. Biophys. Acta.* 1788:2114–2123.

27. Feigenson, G. W. 2009. Phase diagrams and lipid domains in multicomponent lipid bilayer mixtures. *Biochim. Biophys. Acta.* 1788:47–52.

28. Pandit, S. A., E. Jakobsson, and H. L. Scott. 2004. Simulation of the early stages of nano-domain formation in mixed bilayers of sphingomyelin, cholesterol, and dioleylphosphatidylcholine. *Biophys. J.* 87:3312–3322.

29. Rietveld, A., and K. Simons. 1998. The differential miscibility of lipids as the basis for the formation of functional membrane rafts. *Biochim. Biophys. Acta.* 1376:467–479.

30. Mitchell, D. C., and B. J. Litman. 1998. Effect of cholesterol on molecular order and dynamics in highly polyunsaturated phospholipid bilayers. *Biophys. J.* 75:896–908.

31. Fastenberg, M. E., H. Shogomori, …, E. London. 2003. Exclusion of a transmembrane-type peptide from ordered-lipid domains (rafts) detected by fluorescence quenching: extension of quenching analysis to account for the effects of domain size and domain boundaries. *Biochemistry.* 42:12376–12390.

32. Kuzmin, P. I., S. A. Akimov, …, F. S. Cohen. 2005. Line tension and interaction energies of membrane rafts calculated from lipid splay and tilt. *Biophys. J.* 88:1120–1133.

33. García-Sáez, A. J., S. Chiantia, and P. Schwille. 2007. Effect of line tension on the lateral organization of lipid membranes. *J. Biol. Chem.* 282:33537–33544.

34. Honerkamp-Smith, A. R., P. Cicuta, …, S. L. Keller. 2008. Line tensions, correlation lengths, and critical exponents in lipid membranes near critical points. *Biophys. J.* 95:236–246.

35. Tian, A., C. Johnson, …, T. Baumgart. 2007. Line tension at fluid membrane domain boundaries measured by micropipette aspiration. *Phys. Rev. Lett.* 98:208102.

36. Seul, M., and D. Andelman. 1995. Domain shapes and patterns: the phenomenology of modulated phases. *Science.* 267:476–483.

37. Huang, J. 2002. Exploration of molecular interactions in cholesterol superlattices: effect of multibody interactions. *Biophys. J.* 83:1014–1025.